RSC Advances

PAPER

View Article Online
View Journal | View Issue

Cite this: *RSC Adv.*, 2014, 4, 24900

Fe_3O_4/MWCNT as a heterogeneous Fenton catalyst: degradation pathways of tetrabromobisphenol A†

Lincheng Zhou,* He Zhang, Liqin Ji, Yanming Shao and Yanfeng Li

Tetrabromobisphenol A (TBBPA) is the most widely used brominated flame retardant around the world. In this study, we report that iron oxide decorated on a magnetic nanocomposite (Fe_3O_4/MWCNT) was used as a heterogeneous Fenton catalyst for the degradation of TBBPA in the presence of H_2O_2. Fe_3O_4/MWCNT was prepared by a simple solvothermal method, whereby an iron source ($Fe(acac)_3$) and a reductant (*n*-octylamine) were allowed to react in *n*-octanol solvent. Monodisperse Fe_3O_4 nanoparticles of consistent shape were uniformly dispersed on the nanotubes. Samples were characterized by transmission electron microscopy, X-ray diffraction, Fourier transform infrared spectroscopy, X-ray photoelectron spectroscopy, Brunauer–Emmett–Teller surface area measurement, and vibrating sample magnetometry. The samples effectively catalyzed the generation of hydroxyl radicals (·OH) from H_2O_2, which degraded and subsequently mineralized the TBBPA. The whole process took four hours at near neutral pH. A degradation pathway for the system was proposed following analysis of intermediate products by gas chromatography-mass spectrometry. The quantification of Fe^{2+} and Fe^{3+} distribution before and after the recycling test of the composite were explored by X-ray photoelectron spectroscopy, in order to explain the stability and recyclability of the composite. Analysis of the results indicated that the magnetic nanocomposite is a potentially useful and environmentally compatible heterogeneous Fenton's reagent with promising applications related to pollution control.

Received 17th March 2014
Accepted 23rd May 2014

DOI: 10.1039/c4ra02333a

www.rsc.org/advances

1. Introduction

Approximately 60% of all brominated flame retardants contain TBBPA, which is used primarily in printed circuit boards, or as an additive in several types of polymers. In 2004, the global demand for TBBPA was estimated to be 170 000 tons,[1] and China produces about 18 000 tons of the material per year. Despite its reactivity, TBBPA and its metabolites are released into the environment from either products treated with additives, or *via* reactions, and have been identified in samples of air, soil, and sediment,[2] as well as in wastewater.[3] Like most brominated aromatic flame retardants, TBBPA is lipophilic and difficult to degrade, and thus, adversely affects both environmental and biological systems.[4] Therefore, the need to develop an effective method of clearing TBBPA from the environment is significant and urgent. Current methods for the removal of TBBPA from water include adsorption, biological degradation, ozonolysis, and catalytic oxidation.[5–9] Because TBBPA can be broken into small, less toxic or harmless molecules, catalytic degradation is an increasingly important method of controlling this refractory organic pollutant. In 1894 Henry Fenton first reported that alcohols are oxidized in the presence of H_2O_2 and $Fe(H_2O)_6{}^{2+}$.[10] The Fenton system is an attractive catalytic oxidation treatment for effective and exhaustive degradation because of its low cost, lack of toxic reagents (it employs Fe^{2+} and H_2O_2), circumvention of mass transfer limitations due to its homogeneous catalytic nature, and simplicity.[11] However, homogeneous Fenton processes also present certain disadvantages, including a requirement for strong acidity (pH = 3.0), and the formation of a considerable amount of ferric hydroxide sludge during treatment, which requires further separation and disposal.[12–15] Heterogeneous Fenton-like systems using Fe_3O_4 magnetic nanoparticles (MNPs) have been recently developed to overcome problems associated with homogeneous systems. The iron spinel Fe_3O_4 (magnetite) is known for high catalytic activity because it contains Fe^{2+}, which is necessary for the initiation of the Fenton reaction, according to the classical Haber–Weiss mechanism. The octahedral configuration of ions in magnetite confers additional advantages as these sites can easily accommodate both Fe^{2+} or Fe^{3+}, allowing the iron species to be reversibly oxidized and reduced without inducing structural changes.[16] However, while Fe_3O_4 MNPs can be easily separated from the reaction medium under a magnetic field, they also

---

State Key Laboratory of Applied Organic Chemistry, College of Chemistry and Chemical Engineering, Institute of Biochemical Engineering & Environmental Technology, Lanzhou University, Lanzhou 730000, P. R. China. E-mail: zhoulc@lzu.edu.cn; Tel: +86-0931-8912528

† Electronic supplementary information (ESI) available. See DOI: 10.1039/c4ra02333a

tend to aggregate into larger clusters as a result of anisotropic dipolar attractions, which inhibits dispersibility and other properties.[17,18]

Carbon nanotubes (CNT) are a new class of small, adsorbent molecules that exhibit large specific surface areas, with hollow and layered structures. These CNT represent a class of adsorbents that are important for their potential ability to remove many kinds of organic compounds.[19] Studies have demonstrated that CNT act as good supports for Fe_3O_4 MNPs, exhibiting high specific surface areas and low diffusion resistance. Studies have also reported the development of iron oxide/carbon nanostructures.[20–23] For example, Deng *et al.*[23] synthesized Fe_3O_4/MWCNT magnetic nanocomposites and used them as a Fenton-like catalyst to decompose acid orange II. These composites displayed higher activity (90% degradation) than Fe_3O_4 nanocomposites (38% degradation). However, the use of Fe_3O_4/MWCNT magnetic nanocomposites in a heterogeneous Fenton system to catalyze TBBPA degradation has not yet been reported.

In order to implement effective TBBPA degradation, we report in this work the preparation of Fe_3O_4/MWCNT using a simple solvo-thermal method. This new magnetic nanocomposite exhibits improved features, such as improved monodispersion and size control of the Fe_3O_4 nanoparticles on MWCNT, compared to our previous work.[24,25] Moreover, this new Fe_3O_4/MWCNT exhibits high specific surface area and excellent stability, and can be used in a heterogeneous Fenton-like system for TBBPA degradation. Potential mechanisms of the degradation were proposed following analysis by gas chromatography-mass spectrometry (GC-MS).

2. Experimental

2.1. Chemicals and materials

MWCNT (diameter, 10–20 nm) were purchased from Chengdu Organic Chemical Co. Ltd, Chinese Academy of Sciences (AR, Chengdu, China). TBBPA was obtained from Xilong Chemical Co. Ltd (AR, Guangzhou, China). $Fe(acac)_3$ (purity, 99.9%) was purchased from Sigma-Aldrich (AR, United Kingdom). *N*-Octylamine and *n*-octyl alcohol were purchased from Sinopharm Chemical Reagent Co. Ltd (AR, Shanghai, China). The H_2O_2 was purchased from Guangfu Chemical Co. Ltd (30%, Tianjin, China).

2.2. Preparation of Fe_3O_4/MWCNT

The preparation of Fe_3O_4/MWCNT involved a modified solvothermal method in which $Fe(acac)_3$ acted as the iron source, *n*-octylamine acted as the reductant, and *n*-octanol was used as the solvent.[26,27] In a typical experiment, $Fe(acac)_3$ (0.7416 g) and different weights of MWCNT (1.4832 g, 0.7416 g, or 0.3708 g) were mixed with 4 mL *n*-octylamine and 12 mL *n*-octanol. Following ultrasonic dispersion for 1 min (KQ-100, 40 kHz, 100 W), the mixture solution (16 mL) was heated to 110 °C for 1 h, under a flow of nitrogen, to remove trace oxygen and moisture. The pretreatment solution was then transferred to a 50 mL Teflon-lined stainless steel autoclave and heated to 240 °C for 2 h. After cooling to room temperature, the residual solvent was removed by magnetic separation, and the black material was washed thoroughly with ethanol for 12 h in a Soxhlet extractor. Finally, the composite material was dried in a vacuum oven at 30 °C. This process (Scheme 1) produced composites of Fe_3O_4/MWCNT in the following ratios: 1 : 2, 1 : 1 and 2 : 1.

2.3. Instrumentation

The morphology of prepared Fe_3O_4/MWCNT was characterized using a transmission electron microscope (TEM, Tecnai G^2 F30). Powder X-ray diffraction (XRD, Rigaku D/MAX-2400 X-ray diffractometer with Ni-filtered Cu Kα radiation) was used to qualitatively assess the structure of the Fe_3O_4/MWCNT. Fourier transform infrared spectroscopy (FT-IR, American Nicolet Corp. Model 170-SX, using the KBr pellet technique.) and X-ray photoelectron spectroscopy (XPS), were used to verify the composition of the Fe_3O_4/MWCNT. The N_2 adsorption–desorption isotherm was measured at liquid nitrogen temperature (76 K) using a Micromeritics ASAP 2010M instrument. The specific surface area was calculated using the Brunauer–Emmett–Teller (BET) method. Magnetic properties were characterized by vibrating sample magnetometry (VSM, LAKESHORE-7304) at room temperature. The pH of the solutions was determined using a pH meter (HI 9025, HANNA instruments, Romania).

The concentrations of TBBPA were analyzed by HPLC (LC-10AVP Plus, Shimadzu, Japan), equipped with a C-18 column under the following conditions: the mobile phase was an 80 : 20 (v/v) mixture of methanol and water; flow rate, 1.0 mL min^{-1}; detection wavelength, 230 nm; column temperature, 30 °C; and retention time, 9.253 min.

Chemical analyses of the intermediates of TBBPA Fenton degradation were carried out using a GC-MS system (QP2010 Plus, Shimadzu, Japan) equipped with a fused silica capillary column (HP-5MS; length = 30 m; i.d. = 0.25 mm; film thickness = 0.25 μm). The column temperature was programmed as follows: 3 min at 80 °C; a temperature increase of 3 °C min^{-1} up to 300 °C; and 30 min at 300 °C. The helium gas flow rate was 1.0 mL min^{-1}, and the sample size was 2 μL.

2.4. Procedures and analysis

The effects of correlating factors, including pH, H_2O_2 concentration, quality ratio of $Fe(acac)_3$ and MWCNT, and Fe_3O_4/MWCNT concentration, were investigated through batch experiments. The solution pH was adjusted using a minute quantity of 0.1 mol L^{-1} HCl and/or 0.1 mol L^{-1} NaOH. Stock solutions of 100 mg L^{-1} of standardized TBBPA and 180 mmol L^{-1} of H_2O_2 were prepared. Experimental solutions of the desired concentrations were obtained by dilution. The initial

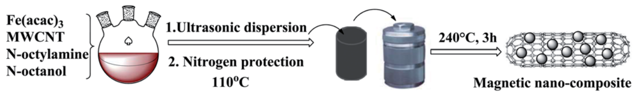

Scheme 1

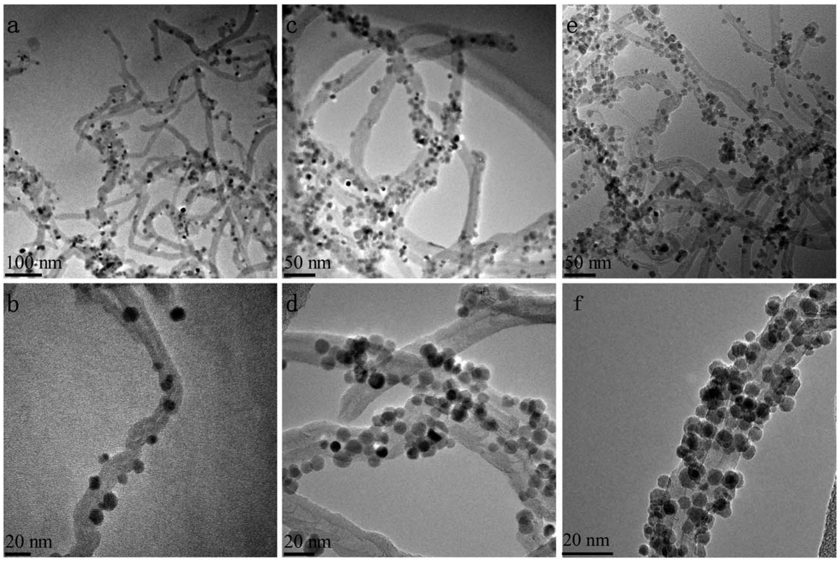

Fig. 1 TEM images of 1 : 2 Fe_3O_4/MWCNT (a and b), 1 : 1 Fe_3O_4/MWCNT (c and d) and 2 : 1 Fe_3O_4/MWCNT (e and f).

concentrations of TBBPA test solutions were 10 mg L^{-1} for all experiments. The appropriate amounts of Fe_3O_4/MWCNT and 10 mL TBBPA solution were added to the reactor, and after thorough mixing, 0.5 mL aliquots of H_2O_2 solution were added every hour. Samples were then transferred to a constant temperature oscillator (150 rpm, 30 °C). After an appropriate time, samples were removed to measure the concentration of TBBPA.

The residue rate of TBBPA (*R*, %) was calculated using eqn (1):

Table 1 The data of surface area, pore volume and pore size for different ratio of Fe_3O_4/MWCNT and pure MWCNT.

Sample	S_{BET} (m^2 g^{-1})	Pore volume (cm^3 g^{-1})	Pore size (nm)
2 : 1 Fe_3O_4/MWCNT	145	0.6911	19.09
1 : 1 Fe_3O_4/MWCNT	164	0.6570	16.07
1 : 2 Fe_3O_4/MWCNT	174	0.6982	16.08
MWCNT	224	1.1771	26.07

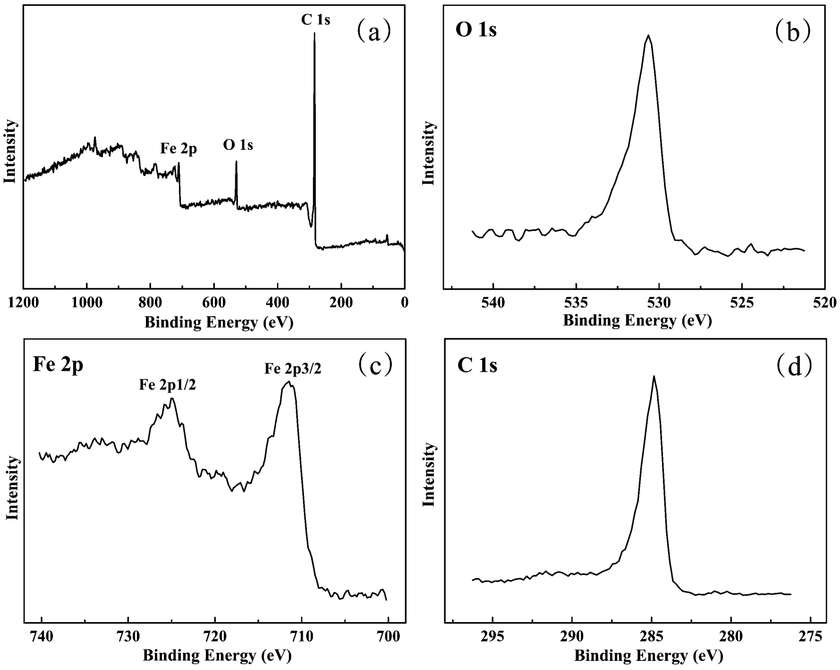

Fig. 2 XPS spectra of 2 : 1 Fe_3O_4/MWCNT. (a) Wide scan, (b) O 1s spectrum, (c) Fe 2p spectrum, (d) C 1s spectrum.

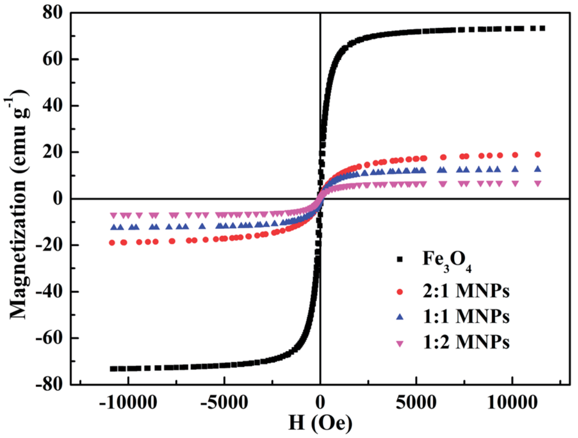

Fig. 3 Magnetic hysteresis curves for different ratios of Fe_3O_4/MWCNT and Fe_3O_4.

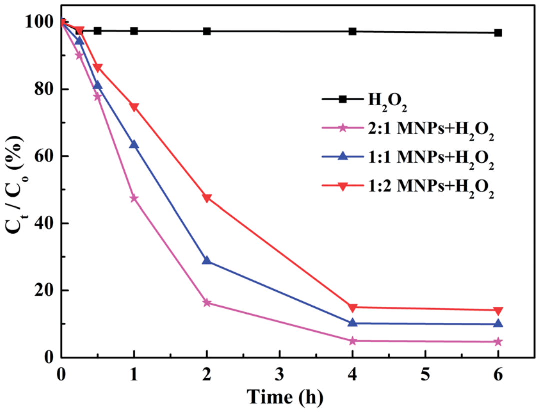

Fig. 4 Effect of quality ratio between $Fe(acac)_3$ and MWCNT on the degradation of TBBPA. Reaction conditions: temperature 303 K; 10 mg L^{-1} TBBPA; 5.0 mg Fe_3O_4/MWCNT; 100 mmol L^{-1} H_2O_2; pH = 5.0.

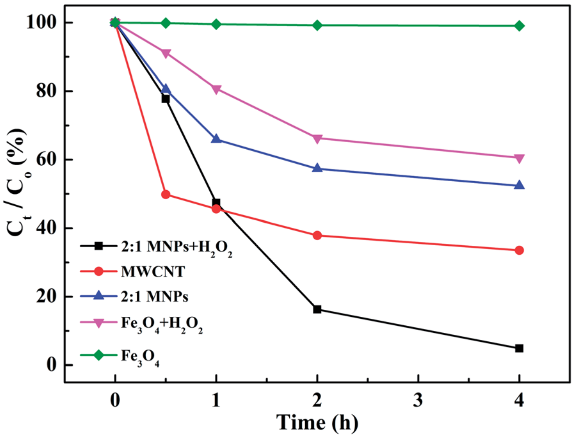

Fig. 5 Degradation and adsorption performance of TBBPA over time under different conditions. Reaction conditions: temperature 303 K; 10 mg L^{-1} TBBPA; 5.0 mg Fe_3O_4/MWCNT, Fe_3O_4 or MWCNT; 100 mmol L^{-1} H_2O_2; pH = 5.0.

$$R = \frac{C_t}{C_0} \times 100\% \qquad (1)$$

where C_0 and C_t are, respectively, the initial and remnant concentrations of TBBPA.

3. Results and discussion

3.1. Characterization of Fe_3O_4/MWCNT

Samples containing Fe_3O_4 and MWCNT at ratios of 1 : 2, 1 : 1, and 2 : 1 were observed by TEM under different magnifications (Fig. 1). Uniform, homogeneous, and non-agglomerated Fe_3O_4 MNPs were found decorated onto the surfaces of the MWCNT. Individual Fe_3O_4 MNPs or MWCNT were not observed, indicating that the preparation method was effective. The use of different ratios of $Fe(acac)_3$ and MWCNT achieved different coverage densities of Fe_3O_4 on the MWCNT. The lowest iron content led to relatively low coverage density by small Fe_3O_4 particles (average diameter 4.19 nm; Fig. 1(a and b)). Increasing the iron content allowed for larger Fe_3O_4 particle growth, so the 1 : 1 Fe_3O_4/MWCNT sample exhibited 5.72 nm Fe_3O_4 particles (Fig. 1(c and d)), while a relatively high coverage density of 6.43 nm Fe_3O_4 particles was achieved in the sample with the highest iron content (Fig. 1(e and f)). The increasing $Fe(acac)_3$ concentration resulted in higher concentrations of Fe_3O_4, which facilitated the thermodynamically stable growth of larger particles.

Fig. S1† shows the XRD patterns of both the pure Fe_3O_4 and the composite. The composite exhibited a different peak at $2\theta = 25.78°$, which can be indexed to the (002) reflection of the graphite structure of the MWCNT.[28] The other peaks represent the pure Fe_3O_4 nanoparticles, as the signals at 30.05°, 35.12°, 43.50°, 54.14°, and 63.01°, are respectively consistent with standard data from the (220), (311), (400), (422), (511), and (440) reflections of the cubic spinel crystal structure of bulk magnetite (JCPDS file no. 19-0629).[29] No obvious peaks from other phases were observed. The main Fe_3O_4 peaks appeared broadened, indicating a very small crystalline portion of the Fe_3O_4 MNPs. According to the full width at half maximum (FWHM) of (311) reflections, the average sizes of the Fe_3O_4 nanocrystalline particles from pure Fe_3O_4 and Fe_3O_4/MWCNT were calculated to be 5.7 nm and 5.9 nm based on the Debye–Scherrer formula, respectively. The almost similar crystallite of bare and decorated Fe_3O_4 suggests that MWCNT can be better support for the growth of metal oxide nanoparticles, without apparent agglomeration.

We observed a signal at 582 cm^{-1} in the FT-IR spectrum related to the Fe–O–Fe stretching vibration of Fe_3O_4[30] and a strong adsorption at 3438 cm^{-1} assigned to O–H stretching of multiwall CNT, which is consistent with previous research indicating a large number of carboxyl and hydroxyl groups on the surface of multiwall CNT (Fig. S2†).[31] Results of the FT-IR indicated that the Fe_3O_4 MNPs were loaded successfully onto the MWCNT.

Samples were also analyzed by XPS (Fig. 2). The wide scan spectrum revealed photoelectron lines at binding energies of approximately 285, 528, and 711 eV (Fig. 2(a)), which were

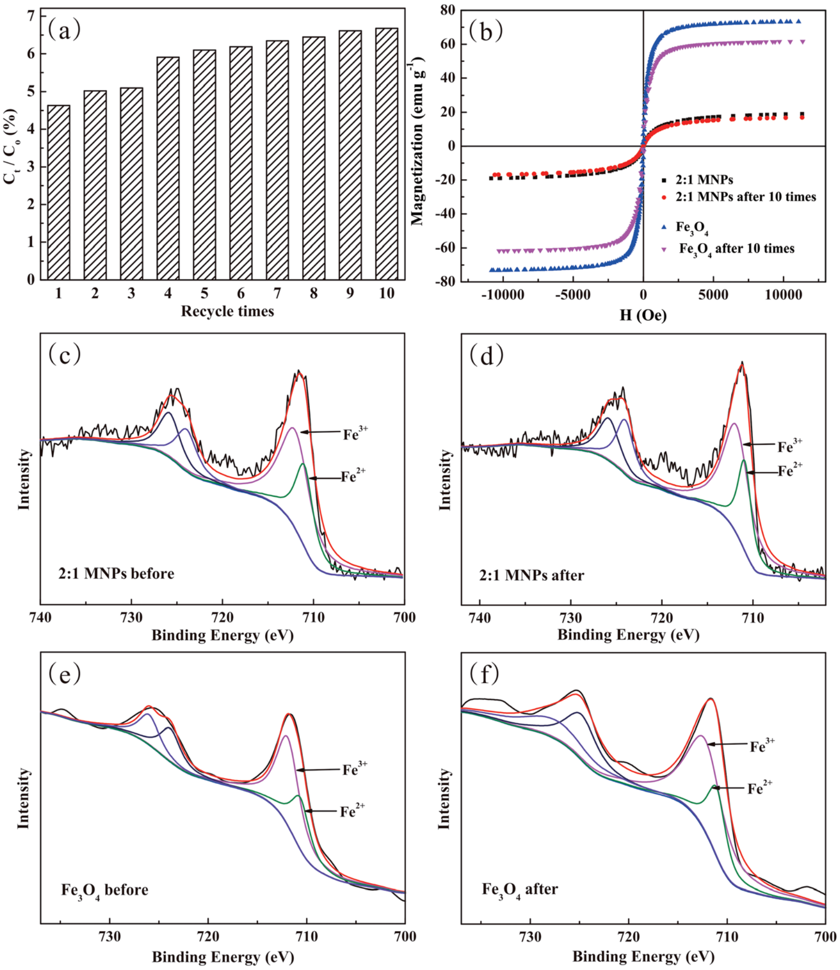

Fig. 6 Catalytic activity of 2 : 1 Fe_3O_4/MWCNT for different cycling numbers (a); magnetic hysteresis curves for 2 : 1 Fe_3O_4/MWCNT and Fe_3O_4 after recycling 10 times (b); XPS spectrum of Fe on 2 : 1 Fe_3O_4/MWCNT before (c) and after (d) degradation of TBBPA; XPS spectrum of Fe on Fe_3O_4 before (e) and after (f) degradation of TBBPA. Reaction conditions in each cycle: temperature 303 K; 10 mg L^{-1} TBBPA; 5.0 mg 2 : 1 Fe_3O_4/MWCNT and Fe_3O_4; 100 mmol L^{-1} H_2O_2; pH = 5.0.

attributed to C 1s, O 1s, and Fe 2p orbitals, respectively. The O 1s spectrum indicates the presence of O 1s (528 eV) from the Fe_3O_4 (Fig. 2(b)).[32] Fe 2p 1/2 and Fe 2p 3/2 peaks were observed at 710 and 725 eV (Fig. 2(c)), further confirming that the oxide in the sample was Fe_3O_4.[33] The electron binding energy of C 1s at 285 eV was attributed to adsorbed carbon in the composites from the MWCNT (Fig. 2(d)).[34]

Nitrogen adsorption–desorption isotherms and pore size distributions were measured for all three samples and pure MWCNT (Fig. S3†). The BET method and Barrett–Joyner–Halenda (BJH) models were used to calculate specific surface area and porosity, respectively. The surface areas, pore volumes, and pore sizes of the different samples are summarized in Table 1. The specific surface area of pure MWCNT was 224 m^2 g^{-1}, and this value decreased with increasing iron content. The high specific surface areas shown by the magnetic CNT (145–174 m^2 g^{-1}) were greater than those of similar materials synthesized by other methods, which did not exceed 120 m^2 g^{-1}.[35,36] Increases in specific surface area resulting from the present solvo-chemical route may be particularly beneficial to the adsorption and degradation of organic pollutants. This observed synergy is believed to result from the adsorptive properties of the support, which increase the rate of substrate degradation. Similar effects were reported by Hu *et al.*[37] who determined that the degradation of pollutants, such as 17α-methyltestosterone, could be accelerated by their adsorption onto multi-walled carbon nanotubes.

The magnetic behaviors of the different Fe_3O_4/MWCNT samples and pure Fe_3O_4 exhibited typical S-type hysteresis loops with no residual magnetism or coercivity (Fig. 3), indicating that the nanoparticles were superparamagnetic. Saturation magnetization for three samples with increasing iron content increased by 6.91, 12.56, and 18.98 emu g^{-1}, which was attributed to the strong magnetic properties of the Fe_3O_4. Although the composites exhibited lower saturation magnetization than pure Fe_3O_4 (73.29 emu g^{-1}), they could still be easily separated from solution using an external magnetic field, which is a useful method for recycling biodegradable materials and reducing the cost of wastewater treatment.

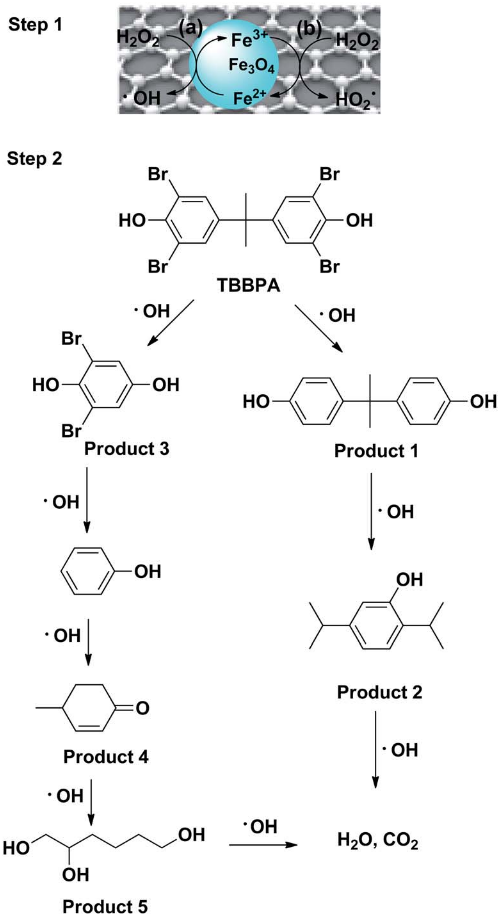

Scheme 2

3.2. Optimization of experimental conditions

3.2.1. Effects of pH. Fenton reactions are very strongly affected by pH. Reactions in a traditional Fenton system proceed smoothly only at pH 3.0.[38] In this study, the degradation of TBBPA was examined at pH 2.0, 3.0, 5.0, 7.0, 9.0, and 11.0 (Fig. S4†). Degradation trends of TBBPA with changing pH were similar for both the composites and the pure Fe_3O_4, with optimal values identified at 5.0 and 3.0, respectively. It is worth mentioning that less than 7.5% of the TBBPA remained at pH < 7.0, indicating that TBBPA was almost completely degraded at or near neutral pH in our Fenton system, and the wide range of conditions under which TBBPA could be degraded demonstrated the efficiency of the composite catalyst.

Two kinds of mechanisms have been proposed to explain the strong oxidization associated with the Fenton reagent. The first mechanism involves the formation of high-valent iron–oxo intermediates, such as $Fe{=}O^{2+}$, as reported by Bray and Gorin in 1932, and as illustrated by eqn (2) and (3) below:[39]

$$Fe^{2+} + H_2O_2 \rightarrow FeO^{2+} + H_2O \quad (2)$$

$$FeO^{2+} + H_2O_2 \rightarrow Fe^{2+} + H_2O + O_2 \quad (3)$$

A related study by Churchill *et al.*[40] reported the synthesis of a new molecular probe capable of detecting Fe^{3+} *via* fluorescence enhancement, which would allow for discrimination between Fe^{2+} and Fe^{3+} during the Fenton reaction. Results of that study confirmed the formation of a ferryl group (FeO^{2+}) as an oxidative intermediate *via* DFT.

The second mechanism is the Haber–Weiss mechanism, which involves the generation of ·OH from H_2O_2 as a key step in the degradation process,[41] as summarized in eqn (4) and (5).

$$Fe^{2+} + H_2O_2 \rightarrow Fe^{3+} + OH^- + \cdot OH \quad (4)$$

$$Fe^{3+} + H_2O_2 \rightarrow Fe^{2+} + H^+ + \cdot OOH \quad (5)$$

While no experimental methods are currently available to distinguish between these two kinds of mechanisms, we selected the latter method for our analysis. At low pH (<3.0) H_2O_2 can form a stable oxonium ion ($H_3O_2^+$), which enhances the scavenging effect of the ·OH,[42,43] and ·OH exhibits a higher oxidation capacity under acidic conditions, thereby inhibiting the decomposition of H_2O_2 into H_2O and O_2.[44] Degradation is also poor under alkali conditions, as this affects the generation of ·OH, and produces hydroxide, which inhibits the catalytic ability of iron.[45,46] Preliminary studies in our laboratory indicated that optimal degradation occurred at pH 5.0, and this pH was maintained for all subsequent degradation experiments.

3.2.2. Effects of H_2O_2 concentration. Increasing H_2O_2 concentration was found to increase TBBPA degradation: TBBPA residue was reduced from 9.7 to 5.3% as H_2O_2 concentration increased from 27 to 54 mmol L^{-1} (Fig. S5†). TBBPA degradation is also directly related to the concentration of ·OH produced by the catalytic decomposition of H_2O_2; therefore, better decomposition is expected when more H_2O_2 is available to produce ·OH. However, full degradation of TBBPA was achieved at the lowest tested concentration, and significant improvements were not affected by increased H_2O_2 concentration. The lack of further improvement at higher concentrations may have been due to hydroxyl radicals scavenging the H_2O_2 (eqn (6) and (7)) and recombining with each other (eqn (8)),[47,48] which may then reduce the rate of degradation.[49]

$$\cdot OH + H_2O_2 \rightarrow HO_2\cdot + H_2O \quad (6)$$

$$\cdot OH + HO_2\cdot \rightarrow O_2 + H_2O \quad (7)$$

$$\cdot OH + \cdot OH \rightarrow H_2O_2 \quad (8)$$

All TBBPA degradation experiments were subsequently conducted using 27 mmol L^{-1} H_2O_2, as this concentration produced the highest degradation.

3.2.3. Effects of catalyst loading. TBBPA degradation was investigated at different loadings (0.0, 0.25, 0.5, 1.0, 2.0, and 4.0 g L^{-1}) as part of the 2 : 1 Fe_3O_4/MWCNT catalyst (Fig. S6†). TBBPA residue rates dropped from 96.3 to 3.2% as the concentration of the composite increased from 0.0 to 4.0 g L^{-1}. This was due to the increased number of active sites on the oxide surface, which accelerated the decomposition of H_2O_2 and the dissolution of iron to produce more ·OH.[37,50] A sharp decrease in TBBPA degradation was observed when the concentration of 2 : 1 Fe_3O_4/MWCNT was lower than 0.5 g L^{-1}, while only slight changes were observed when the concentration of 2 : 1 Fe_3O_4/MWCNT exceeded 0.5 g L^{-1}. However, at 0.5 g L^{-1}, TBBPA could be removed almost completely, so 0.5 g L^{-1} of 2 : 1 Fe_3O_4/MWCNT was used in subsequent experiments.

3.2.4. Effects of iron content. The different Fe_3O_4/MWCNT samples were prepared at different quality ratios of Fe(acac)$_3$ and MWCNT (1 : 2, 1 : 1, and 2 : 1), and their abilities to degrade TBBPA were compared (Fig. 4). Improved degradation was observed with increasing iron content, as the three samples exhibited decreasing residue rates of 23.26, 11.13, and 4.65%, respectively. The increased activity of the composites, resulting from increased iron content, was attributed to an increase in the number of active sites, which are visible in the TEM (Fig. 1). This reaction was considered a pseudo-first-order reaction, with the concentration C_t of TBBPA at reaction time t being described as follows:[51]

$$C_t = C_0 \exp(-kt) \tag{9}$$

where C_0 was the initial concentration of TBBPA, and k was the pseudo first-order rate constant. Logarithmic plots of the concentration of TBBPA as a function of degradation time appear as well-behaved straight lines ($R^2 > 0.98$), indicating that the degradation reaction was pseudo-first-order. The rate constant k was calculated from the slope of the line, while values of 0.0061, 0.0098, and 0.0132 min^{-1} were calculated for the three samples by increasing iron content, respectively. Each of these values was greater than the 1.8×10^{-4} min^{-1} reported for a $Fe_{2.02}Ti_{0.98}O_4/H_2O_2$ system for the degradation of TBBPA.[52]

3.3. TBBPA degradation experiments by heterogeneous Fenton reaction

The catalytic degradation efficiencies of TBBPA by 2 : 1 Fe_3O_4/MWCNT and Fe_3O_4 were evaluated under optimal conditions. In order to differentiate between degradation and adsorption, adsorption tests were also conducted using the three kinds of materials (2 : 1 Fe_3O_4/MWCNT, pure Fe_3O_4 and pure MWCNT). As seen in Fig. 5, the adsorption of TBBPA was almost negligible in the presence of pure Fe_3O_4, which might have been due to its low surface areas. The increased surfaces areas of both 2 : 1 Fe_3O_4/MWCNT and pure MWCNT resulted in predictable increases in adsorption performance, with TBBPA residual rates of 52.34 and 33.55%, respectively. However, when H_2O_2 was added, The TBBPA residual rate for 2 : 1 Fe_3O_4/MWCNT dropped to 4.87%, while the TBBPA rate when pure Fe_3O_4 was used as a catalyst for TBBPA degradation was 60.56%. These comparisons were made based on equal weights of the catalysts. Results of these experiments indicated that the degradation efficiency of 2 : 1 Fe_3O_4/MWCNT was two times higher than that of Fe_3O_4, and that approximately twice as much TBBPA was degraded as adsorbed. This significant activity enhancement can be attributed to homogeneous dispersion of the Fe_3O_4 nanoparticles, which appears to increase the number of active sites for substrate access.

3.4. Stability of Fe_3O_4/MWCNT

The stability and recyclability of both 2 : 1 Fe_3O_4/MWCNT and pure Fe_3O_4 were evaluated *via* their successive use in TBBPA degradation (Fig. 6). After 10 cycles, the TBBPA residual rate remained at 6.8% (Fig. 6(a)), and the saturation magnetization of composite after 10 cycles was 16.93 emu g^{-1} (Fig. 6(b)), which represented only a 1.1% decrease from its original value. By contrast, the saturation magnetization of pure Fe_3O_4 after 10 cycles was 61.69 emu g^{-1} (Fig. 6(b)), which represented a 15.8% decrease from its original value. To further demonstrate the stability of the structures, XPS was used to analyze the catalysts before and after the Fenton reaction. The details of the Fe 2p peaks (Fe 2p 1/2 and Fe 2p 3/2) of the 2 : 1 Fe_3O_4/MWCNT and pure Fe_3O_4 before and after their use during TBBPA degradation are presented in Fig. 6(c–f) and Table S1.† The Fe 2p 1/2 peak for Fe_3O_4 was deconvoluted into the Fe^{3+} and Fe^{2+} peaks. Before use, the corresponding binding energy values were 712.00 eV and 711.00 eV, respectively (Fig. 6(c)), and these values did not change significantly after 10 cycles of use for TBBPA degradation (711.80 eV and 710.90 eV: Fig. 6(d)). Calculation of the peak areas indicated that 67.6% of the total iron surface atoms were Fe^{3+}, while 32.4% were in the Fe^{2+} state, which was consistent with the Fe_3O_4 crystal structure. For samples evaluated after 10 cycles of TBBPA degradation, the concentration of Fe^{3+} on the surface increased to 70.0%, while Fe^{2+} decreased to 30.0%, which indicated that some of the Fe^{2+} on the outermost layer of the catalyst was oxidized into Fe^{3+} during the Fenton reaction. Meanwhile, we used the same methods to analyze the pure Fe_3O_4. Before use, the corresponding binding energy values were 711.91 eV and 710.62 eV, respectively (Fig. 6(e)). After 10 cycles of use for TBBPA degradation, these values were 712.20 eV and 711.05 eV (Fig. 6(f)). Fe^{2+} surface concentration was 32.7% in the pure Fe_3O_4 before use, but only 27.8% after use. It is well known that the oxidation of the ferrous iron by H_2O_2 is much faster than the reduction of the ferric iron by H_2O_2. Thus, in order to speed up the redox cycle between ferrous and ferric species, it should improve the reduction of the ferric iron by H_2O_2.[23] Obviously, the reduction of the ferric iron in the Fenton system use Fe_3O_4/MWCNT was more efficient than use pure Fe_3O_4. Collectively, these results suggested excellent stability and durability of the composite.

3.5. Reaction mechanism

The mechanism of this Fenton system was investigated *via* GC-MS analysis of the products of degradation after 4 h. Five main intermediate products were detected, and their likely molecular structures and fragment ion peaks are summarized in Table S2.† A proposed mechanism associated with this reaction is presented in Scheme 2.[53] In this scheme, path (a) illustrates the conversion of H_2O_2 to OH^- and $\cdot OH$ in the presence of Fe^{2+}, which was generated on the surface of Fe_3O_4 MNPs. Path (b) illustrates the transformation of Fe^{3+} on the surface of Fe_3O_4 MNPs to Fe^{2+}. In subsequent pathway, the TBBPA was oxidized into intermediates **1–5** by the activated $\cdot OH$. Product **1** was identified as bisphenol A, which resulted from the oxidation of TBBPA by $\cdot OH$ and the loss of its Br atoms.[52] The presence of product **2** likely resulted from the reaction of ·OH with product **1**. Homolytic cleavage of the C–C bond between the quaternary carbon and the aromatic ring in TBBPA was responsible for the creation of product **3**. Phenol may have resulted from the oxidation of product **3** by ·OH. Additionally, the phenol might then have been oxidized into product **4**, which was further oxidized (following ring opening) to generate open chain alcohols, such as product **5**. All the intermediates could eventually be mineralized into H_2O and CO_2.[54] The proposed mechanism suggests that the composite exhibits good activity and high specific surface area, which provides a great activated surface for the Fenton system,[22,55] and that the Fe_3O_4 MNPs may provide sufficient electrons to facilitate the degradation reactions.[22,50]

4. Conclusions

In our work, Fe_3O_4/MWCNT catalysts were prepared using a modified solvothermal method. Shape-controlled and monodisperse Fe_3O_4 nanoparticles were found to be uniformly dispersed on the MWCNT. The resulting high activity was attributed to the Fe_3O_4 nanoparticles' narrow size distribution, and good dispersion on MWCNT. The specific surface area exhibited by the composites was 145 $m^2\ g^{-1}$, which increased the number of available active sites for MWCNT access, and improved degradation. The composites were then used as heterogeneous Fenton reagents to catalyze the degradation of TBBPA by H_2O_2. Degradation was optimized at pH 5.0 using 0.5 $g\ L^{-1}$ catalyst and 27 mmol L^{-1} H_2O_2. The detailed XPS studies of composite and pure Fe_3O_4 indicated that the composite was stable and retained strong activity after 10 cycles of reuse. The ability of the catalyst to degrade TBBPA at near neutral pH, and it's excellent stability and activity, suggest that it may have many useful applications. Careful analysis of the main intermediate products for this reaction led to a proposed mechanism of TBBPA degradation, which suggested multiple pathways of action on TBBPA by hydroxyl radicals.

Acknowledgements

The authors would like to acknowledge the financial support for this study provided by the Fundamental Research Funds for the Central Universities (lzujbky-2013-65) and the National Science Foundation for Fostering Talents in Basic Research, of the National Natural Science Foundation of China (Grant no. J1103307).

References

1 M. S. E. Mäkinen, M. R. A. Mäkinen, J. T. B. Koistinen, A. L. Pasanen, P. O. Pasanen, P. J. Kalliokoski and A. M. Korpi, *Environ. Sci. Technol.*, 2009, **43**, 941–947.
2 L. S. Birnbaum and D. F. Staskal, *Environ. Health Perspect.*, 2003, **112**, 9–17.
3 E. Blanco, M. C. Casais, M. C. Mejuto and R. Cela, *J. Chromatogr. A*, 2005, **1071**, 205–211.
4 S. Strack, T. Detzel, M. Wahl, B. Kuch and H. F. Krug, *Chemosphere*, 2007, **67**, S405–S411.
5 I. I. Fasfous, E. S. Radwan and J. N. Dawoud, *Appl. Surf. Sci.*, 2010, **256**, 7246–7252.
6 J. Xu, W. Meng, Y. Zhang, L. Li and C. Guo, *Appl. Catal., B*, 2011, **107**, 355–362.
7 B. Uhnakova, R. Ludwig, J. Peknicova, L. Homolka, L. Lisa, M. Sulc, A. Petrickova, F. Elzeinova, H. Pelantova, D. Monti, V. Kren, D. Haltrich and L. Martinkova, *Bioresour. Technol.*, 2011, **102**, 409–9415.
8 S. K. Han, P. Bilski, B. Karriker, R. H. Sik and C. F. Chignell, *Environ. Sci. Technol.*, 2008, **42**, 166–172.
9 I. Ioan, S. Wilson, E. Lundanes and A. Neculai, *J. Hazard. Mater.*, 2007, **142**, 559–563.
10 H. H. Fenton, *J. Chem. Soc., Trans.*, 1894, **65**, 899–910.
11 S. Esplugas, J. Giménez, S. Contreras, E. Pascual and M. Rodríguez, *Water Res.*, 2002, **36**, 1034–1042.
12 L. Gomathi Devi, K. S. Anantha Raju and S. Girish Kumar, *J. Environ. Monit.*, 2009, **11**, 1397–1404.
13 L. Gomathi Devi, S. Girish Kumar and K. Mohan Reddy, *Cent. Eur. J. Chem.*, 2009, **7**, 468–477.
14 R. C. Costa, M. F. Lelis, L. C. Oliveira, J. D. Fabris, J. D. Ardisson, R. R. Rios, C. N. Silva and R. M. Lago, *J. Hazard. Mater.*, 2006, **129**, 171–178.
15 A. Cuzzola, M. Bernini and P. Salvadori, *Appl. Catal., B*, 2002, **36**, 231–237.
16 P. V. Nidheesha, R. Gandhimathi, S. Velmathib and N. S. Sanjinib, *RSC Adv.*, 2014, **4**, 5698–5708.
17 D. K. Yi, S. S. Lee and J. Y. Ying, *Chem. Mater.*, 2006, **18**, 2459–2461.
18 A. H. Lu, W. C. Li, N. Matoussevitch, B. Spliethoff, H. Bonnemann and F. Schuth, *Chem. Commun.*, 2005, 98–100.
19 J. L. Gong, B. Wang, G. M. Zeng, C. P. Yang, C. G. Niu, Q. Y. Niu, W. J. Zhou and Y. Liang, *J. Hazard. Mater.*, 2009, **164**, 1517–1522.
20 H. C. Zhang, M. Hai, S. Y. Lian, H. Hui, H. T. Li, L. L. Zhang, Y. Liu, Z. H. Kang and S. T. Lee, *Dalton Trans.*, 2011, **40**, 10822–10825.
21 B. Y. Yu and S. Y. Kwak, *J. Mater. Chem.*, 2012, **22**, 8345–8353.
22 Q. Liao, J. Sun and L. Gao, *Colloids Surf., A*, 2009, **345**, 95–100.
23 J. Deng, X. Wen and Q. Wang, *Mater. Res. Bull.*, 2012, **47**, 3369–3376.
24 L. Q. Ji, L. C. Zhou, X. Bai, Y. M. Shao, G. H. Zhao, Y. Z. Qu and Y. F. Li, *J. Mater. Chem.*, 2012, **22**, 15853–15862.
25 L. C. Zhou, L. Q. Ji, P. C. Ma, Y. M. Shao, H. Zhang, W. J. Gao and Y. F. Li, *J. Hazard. Mater.*, 2014, **265**, 104–114.
26 Y. Tian, B. Yu, X. Li and K. Li, *J. Mater. Chem.*, 2011, **21**, 2476–2481.
27 J. Wan, W. Cai, J. Feng, X. Meng and E. Liu, *J. Mater. Chem.*, 2007, **17**, 1188–1192.
28 B. Jia and L. Gao, *J. Phys. Chem. B*, 2007, **111**, 5337–5343.
29 D. Caruntu, G. Caruntu, Y. Chen, C. J. O'Connor, G. Goloverda and V. L. Kolesnichenko, *Chem. Mater.*, 2004, **16**, 5527–5534.
30 Y. Liu, W. Jiang, Y. Wang, X. J. Zhang, D. Song and F. S. Li, *J. Magn. Magn. Mater.*, 2009, **321**, 408–412.

31 M. Yamaura, R. L. Camilo, L. C. Sampaio, M. A. Macêdo, M. Nakamura and H. E. Toma, *J. Magn. Magn. Mater.*, 2004, **279**, 210–217.

32 W. Wu, Q. He, H. Chen, J. Tang and L. Nie, *Nanotechnology*, 2007, **18**, 145609.

33 T. Missana, C. Maffiotte and M. García-Gutiérrez, *J. Colloid Interface Sci.*, 2003, **261**, 154–160.

34 S. Cui, X. Shen, B. Lin, G. Jiang and W. Zhang, *J. Wuhan Univ. Technol., Mater. Sci. Ed.*, 2008, **23**, 436–439.

35 A. K. Mishra and S. Ramaprabhu, *Energy Environ. Sci.*, 2011, **4**, 889–895.

36 C. Zhang, J. Sui, J. Li, Y. Tang and W. Cai, *Chem. Eng. J.*, 2012, **210**, 45–52.

37 X. Hu, B. Liu, Y. Deng, H. Chen, S. Luo, C. Sun, P. Yang and S. Yang, *Appl. Catal., B*, 2011, **107**, 274–283.

38 J. J. Pignatello, E. Oliveros and A. MacKay, *Crit. Rev. Environ. Sci. Technol.*, 2006, **36**, 1–84.

39 W. C. Bray and M. H. Gorin, *J. Am. Chem. Soc.*, 1932, **54**, 2124–2125.

40 D. P. Murale, S. T. Manjare, Y. S. Lee and D. G. Churchill, *Chem. Commun.*, 2014, **50**, 359–361.

41 F. Haber and J. Weiss, *Proc. R. Soc. London, Ser. A*, 1934, **861**, 332–351.

42 J. H. Sun, S. P. Sun, M. H. Fan, H. Q. Guo, Y. F. Lee and R. X. Sun, *J. Hazard. Mater.*, 2008, **153**, 187–193.

43 L. Gomathi Devi, S. Girish Kumar, K. Mohan Reddy and C. Munikrishnappa, *J. Hazard. Mater.*, 2009, **164**, 459–467.

44 P. Bautista, A. F. Mohedano, J. A. Casas, J. A. Zazo and J. J. Rodriguez, *J. Chem. Technol. Biotechnol.*, 2008, **83**, 1323–1338.

45 L. Gomathi Devi, K. S. Anantha Raju, S. Girish Kumar and K. Eraiah Rajashekhar, *J. Taiwan Inst. Chem. Eng.*, 2011, **42**, 341–349.

46 J. Zhang, J. Zhuang, L. Gao, Y. Zhang, N. Gu, J. Feng, D. Yang, J. Zhu and X. Yan, *Chemosphere*, 2008, **73**, 1524–1528.

47 R. V. Solomon, I. S. Lydia, J. P. Merlin and P. Venuvanalingam, *J. Iran. Chem. Soc.*, 2012, **9**, 101–109.

48 S. Girish Kumar and L. Gomathi Devi, *J. Phys. Chem. A*, 2011, **115**, 13211–13241.

49 S. H. Tian, Y. T. Tu, D. S. Chen, X. Chen and Y. Xiong, *Chem. Eng. J.*, 2011, **169**, 31–37.

50 L. Xu and J. Wang, *Appl. Catal., B*, 2012, **123–124**, 117–126.

51 M. Zhu and G. Diao, *J. Phys. Chem. C*, 2011, **115**, 18923–18934.

52 Y. Zhong, X. Liang, Y. Zhong, J. Zhu, S. Zhu, P. Yuan, H. He and J. Zhang, *Water Res.*, 2012, **46**, 4633–4644.

53 S. Zhang, X. Zhao, H. Niu, Y. Shi, Y. Cai and G. Jiang, *J. Hazard. Mater.*, 2009, **167**, 560–566.

54 P. Shi, R. Su, S. Zhu, M. Zhu, D. Li and S. Xu, *J. Hazard. Mater.*, 2012, **229–230**, 331–339.

55 F. Peng, X. B. Fu, H. Yu and H. J. Wang, *New Carbon Mater.*, 2007, **22**, 213–217.